CORA Cork Open Research Archive
Cartlann Taighde Oscailte Chorcaí

Title	Diameter controlled germanium nanowires with lamellar twinning and polytypes
Authors	Biswas, Subhajit;Doherty, Jessica;Majumdar, Dipanwita;Ghoshal, Tandra;Rahme, Kamil;Conroy, Michele;Singha, Achintya;Morris, Michael A.;Holmes, Justin D.
Publication date	2015-04-16
Original Citation	BISWAS, S., DOHERTY, J., MAJUMDAR, D., GHOSHAL, T., RAHME, K., CONROY, M., SINGHA, A., MORRIS, M. A. & HOLMES, J. D. 2015. Diameter-Controlled Germanium Nanowires with Lamellar Twinning and Polytypes. Chemistry of Materials, 27, 3408-3416. http://dx.doi.org/10.1021/acs.chemmater.5b00697
Type of publication	Article (peer-reviewed)
Link to publisher's version	http://pubs.acs.org/journal/cmatex - 10.1021/acs.chemmater.5b00697
Rights	© American Chemical Society, 2015. This document is the Accepted Manuscript version of a Published Work that appeared in final form in Chemistry of Materials, copyright © American Chemical Society after peer review and technical editing by the publisher. doi: 10.1021/acs.chemmater.5b00697
Download date	2026-11-12 01:00:33
Item downloaded from	https://hdl.handle.net/10468/2226

UCC
University College Cork, Ireland
Coláiste na hOllscoile Corcaigh

Diameter Controlled Germanium Nanowires with Lamellar Twinning and Polytypes

Subhajit Biswas[†*], *Jessica Doherty*[†], *Dipanwita Majumdar*[#], *Tandra Ghoshal*[†], *Kamil Rahme*[§], *Michelle Conroy*[†], *Achintya Singha*[#], *Michael A. Morris*[†ϕ] *and Justin D. Holmes*[†ϕ*]

[†]Materials Chemistry & Analysis Group, Department of Chemistry and the Tyndall National Institute, University College Cork, Cork, Ireland. [ϕ]AMBER@CRANN, Trinity College Dublin, Dublin 2, Ireland. [#] Department of Physics, Bose Institute, Kolkata-700009, India. [§]Department of Sciences, Faculty of Natural and Applied Science, Norte Dame University (Louaize), Zouk Mosbeh, Lebanon.

RECEIVED DATE (to be automatically inserted after your manuscript is accepted if required according to the journal that you are submitting your paper to)

*To whom correspondence should be addressed: Tel: +353 (0)21 4903608; Fax: +353 (0)21 4274097; E-mail: j.holmes@ucc.ie (JDH) and s.biswas@ucc.ie (SB)

ABSTRACT: One-dimensional nanostructures with controllable morphologies and defects are appealing for use in nanowire devices. This paper details the influence of colloidal magnetite iron oxide nanoparticle seeds to regulate the radial dimension and twin boundary formation in Ge nanowires grown through a liquid-injection chemical vapor deposition process. Control over the mean nanowire diameter, even in the sub-10 nm regime, was achieved due to the minimal expansion and aggregation of iron oxide nanoparticles during the growth process. The uncommon occurrence of heterogeneously distributed multiple layer {111} twins, directed perpendicular to the nanowire growth axis, were also observed in <111>-directed Ge nanowires, especially those synthesized from patterned hemispherical Fe_3O_4 nanodot catalysts. Consecutive twin planes along <111>-oriented nanowires resulted in a local phase transformation from 3C diamond cubic to hexagonal 4H allotrope. Localized polytypic crystal phase heretostructures were formed along <111>-oriented Ge nanowire using magnetite nanodot catalysts.

Keywords: Nanowires, germanium, vapor-solid-solid growth, twin boundaries, polytype

Introduction

Semiconductor nanowires have great commercial potential as components in a vast range of applications, including chemical and biological sensing, computing, optoelectronics and photovoltaic devices.[1-8] The integration of semiconductor nanowires into device geometries[9] requires control over their morphology, dimensions, growth orientation, crystal phase and structural defects. Catalytic bottom-up approaches, such as vapor-liquid-solid (VLS)[10-12], vapor-solid-solid (VSS)[13-14], supercritical fluid-liquid-solid (SFLS)[15-17] techniques, are popular routes for growing high-aspect ratio one-dimensional nanostructures[18-19], where

nanowire diameters can be controlled by the dimension of the catalysts.[20] Control over nanowire diameters, in turn, facilitates regulation over their growth orientation.[21] However, difficulty arises in the precise control of nanowire diameters at high temperatures (> 350 °C), due to prominent surface diffusion of many catalytic metals during nanowire growth. Surface diffusion of nanoparticle catalysts can initiate at relatively low temperatures compared to their counterparts, due to melting point depression of nanoscale catalysts.[22] Various templating methods, such as anodic aluminium oxide (AAO), silica membranes and metal assisted etching (MAE) have been employed to grow nanowires with thin and uniform diameters.[23-25] However releasing nanowires from templates often requires harsh chemical treatments, which also damages the surfaces of the nanowires. Superior control over Si and Ge nanowire diameters, with sub-20 nm dimensions, has been reported from solid metal seeds in sub-eutectic, VSS-like growth processes[14, 20, 26]. Sub-eutectic metal catalysts, such as Ni, Co, Pt, Fe, used for Si or Ge nanowire growth, have high melting points and are therefore resistant to pronounced surface diffusion during nanowire growth. However, VSS-growth of Si and Ge nanowires regularly results in the formation of stable metal silicide and germanide alloys respectively, leading to an increase in the lattice volume of the nucleating seed. An expansion of the catalyst seed ultimately leads to an increase in the mean diameter of the nanowires synthesized.

Nanowires of uniform morphology, *i.e.* with narrow diameter distributions and a single growth orientation, are desirable for precision integration of bottom-up grown nanowires into devices. Additionally, nanowires with inhomogeneous heterostructures and periodic twin boundaries are attracting attention as components for optical, electrical and thermophysical applications.[27-29] The control of twin periodicity in group IV nanowires, especially Ge, offers the possibility of band structure engineering[30-31] and the modulation of thermoelectric

properties through modulated side faceting.[29] Inhomogeneous stress fields caused by twinning and surface faceting can locally affect the conduction and valence band potential thus altering electronic band structure.[32] Periodic twinned planes in semiconductor nanowires can also generate polytype superstructures, where stacking faults in the *abc* stacking sequence, along the <111> direction, can produce local hexagonal ordering in a cubic crystal; for example *aba* packing, leading to polytypes with distinctly unique optical and electrical properties.[27, 33-34] The generation of controlled twinned and polytype defects within individual nanowires allows the realization of heterostructures from a single component semiconductor, with perfect lattice matching and preserved interface bonds. These polytype nanowire structures potentially augment electron scattering at the interfaces between the different crystal phases, permitting the formation of superlattice states as the Bloch wave functions in the two adjacent layers are quite different due to different band structure and crystal orientation.

Fabrication of <111> oriented group IV twinned nanowires, where the lateral twin boundaries run perpendicular to the nanowire growth axis and the induction of different polytypes along the length of a single group IV nanowire are challenging. Although a remarkable degree of control of twinning and polytype generation has been demonstrated in III-V nanowires[35-36], polytype and lateral twin superstructure formation is still a challenge in group IV nanowires[37], where only longitudinal {111} twin boundaries are formed in <112>-directed nanowires.[16, 38] Lateral twin planes and polytype crystal phases have been generated in Si nanowires by catalytic bottom-up growth by manipulating process constrains such as innovative catalysts, precursor partial pressure and surface stress[39-41], but twin plane and polytype formation is not so common for Ge nanowires. Only recently, 2H polytypes of Ge (although not perpendicular to the growth axis) have been formed through post-growth

thermomechanical treatment.[42] Periodic twinning in Ge is particularly interesting as such structures can lead to folding-mediated direct optical transitions in indirect semiconductors.[43] Here we report the use of magnetite iron oxide (Fe_3O_4) nanoparticle catalysts to synthesize diameter-controlled Ge nanowire in the sub-20 nm range. These nanoparticles retained their size during nanowire growth with negligible surface diffusion and expansion of growth promoters, thus enabling the growth of Ge nanowires with a similar diameter range to the nanoparticle catalysts. The use of these magnetite nanoparticle catalysts, particularly hemi-spherical shaped nanodots fabricated through block co-polymer lithography, were used to produce nanowires with lateral twin planes perpendicular to the growth direction, resulting localized hexagonal polytypes in the nanowires.

Results & Discussion

Ge nanowires were grown from colloidal magnetite nanoparticle catalysts with three different diameters; 7.2 (±1.2), 14 (±1.9) and 21.5 (±3.2) nm. Size-monodisperse Fe_3O_4 nanoparticles were prepared from iron chloride and sodium oleate in a two-step synthesis process, involving the thermal decomposition of the organometallic complex of iron-oleate at different temperatures (see Experimental Section in Supporting Information for the detailed nanoparticle synthetic method).[44] Oleic acid was used as a reducing agent and the intermediate capping ligand, with different proportions of the iron-oleate organometallic complex used for the synthesis of the differently sized Fe_3O_4 nanoparticles. A transmission electron microscope (TEM) image of the smallest Fe_3O_4 nanoparticles produced (~ 7 nm) is shown in Figure 1(a), confirming the size-monodispersity and mean diameter of the particles. The diameter distributions shown in Figure 1(b) validate the relatively narrow spread of radial dimensions for the different nanoparticles. Inter-planar spacing obtained from selected area electron diffraction (SAED) patterns (inset of Figure 1(a)) matches well with the lattice

spacing of magnetite iron oxide with a cubic symmetry. These small colloidal magnetite nanoparticles were deposited onto silicon (001) substrates (no native oxide removal procedure was applied on the substrate prior to growth) and dried at 180 °C under vacuum. A liquid injection chemical vapor deposition (LICVD) technique[45], using toluene as the solvent phase, was adopted for growing the Ge nanowires on the surface of Si (001) substrates. Diphenylgermane (DPG) was used as the Ge source in the reactions and the nanoparticle concentration in each case was fixed at 90 μmole cm^{-3}. Nanowire growth temperature was fixed at 460 °C, to ensure sufficient seeding of Ge nanowires from Fe_3O_4 catalyst particles through a VSS mechanism (a detailed synthetic procedure for Ge nanowire growth is described in Experimental Section of Supporting Information). Very high growth temperatures were avoided to prevent the formation of an amorphous carbon shell around the nanowires and the uncontrolled homogeneous nucleation of Ge particles, due to the kinetically enhanced thermal decomposition of germanium precursor.

Diameter Controlled Nanowires: The scanning electron microscopy (SEM) image shown in Figure 2(a) shows the growth of Ge nanowires from Fe_3O_4 nanoparticle seeds with a mean diameter of 14 nm. The SEM image in the inset of Figure 2(a) highlights the uniformity in the radial dimensions of the nanowires, with negligible formation of particulates due to homogeneous nucleation. A narrow Ge nanowire diameter distribution (determined from TEM analysis of ~ 100 nanowires) of 16 (±5.1) nm is depicted in the inset of Figure 2(a), for nanowires grown from Fe_3O_4 seeds with a mean diameter of 14 ((±1.9) nm. The slight increase in the mean diameter and the width distribution of the Ge nanowires grown from Fe_3O_4 nanoparticle catalysts, emphasizes the superior size retention of the nanoparticles during nanowire growth. The crystalline quality of the Ge nanowires was confirmed by the high-resolution TEM, as shown in Figure 2 (b). Most of the nanowires synthesized from the

colloidal Fe_3O_4 seeds had smooth surfaces and were highly crystalline with low defect densities, *i.e.* < 5 % of nanowires examined showed multiple twins. Nanowires were crystallized with a diamond-cubic structure (JCPDS cards #04-0545), where the preferred growth directions for the nanowires were <110>, as determined from TEM and Fast Fourier Transform (FFT) pattern analysis (a particular example is shown in Figure 2(b)). Greater than 75 % of the Ge nanowires produced in this part of the study were oriented along the [110] growth axis; the most commonly observed growth orientation for nanowires below 20 nm.[21, 46] Previously reported Fe_2O_3-seeded Ge nanowires grown under supercritical conditions described an equal proportion of <110> and <111> directed nanowires.[47] Differences in the crystal growth directions of Ge nanowires grown from Fe_2O_3 nanoparticles, as opposed to Fe_3O_4 seeds used in this study, probably relates to variances in the solid phase seeding mechanism, a different diameter regime and the morphologies of the catalyst-nanowire interfaces. The crystal structure of the catalyst and the interfaces between the seed and the growing nanowire strongly influences the surface energies at the growth interface, leading to nanowires within a certain growth direction. Although the energy and morphology of the interface for the solid phase seeding of Ge nanowires with Fe_3O_4 nanoparticles is entirely different from conventional Au seeded VLS nanowire growth, a surprising similarity in the diameter dependent nanowire growth orientation is observed with Au seeded Si nanowires. A few <111> oriented nanowires (~2-3 %) showed modulated contrast patterns in the bright-filed TEM image (shown in the inset of Figure 2 (b)) along the lengths of the nanowires. The changes in the contrast are due to the altered orientation of the nanowire segments relative to the impinging electron beam. TEM observations (Figure S1 in Supporting Information) confirms the occurrence of {111} twin boundaries perpendicular to the nanowire <111> growth direction. Of note, is the similarity between the initial diameter of our Fe_3O_4 nanoparticle seeds (mean diameter ~14 nm) and the widths of Ge nanowires

grown from them (mean diameter ~16 nm). The sub-eutectic growth of Ge nanowires from metal seeds such as Ni or Fe typically results in the formation of large diameter wires, due to the volume expansion of the nanoparticles by 300-400 % upon Ge uptake and the formation of a germanide phase.[20] The use of magnetite iron oxide nanoparticles helps to minimize this expansion, allowing nanowires with a mean diameter similar to catalytic seeds. Also, Fe_3O_4 catalytic seeds not only participate in guiding one-dimensional growth of Ge, but also enable precursor decomposition[48], thus promoting nanowire formation from non-reactive organometallic precursors at lower temperatures.

To confirm the phase of the catalyst at the tip of the nanowires after the growth, energy dispersive X-ray (EDX) analysis in dark field scanning transmission electron microscopy (STEM), TEM and FFT analysis were performed on the metallic components at the tips of the nanowires (Figure 3). An EDX spectrum (Figure 3 (a)) recorded from the catalyst tip of a nanowire agrees well with the formation of the $FeGe_2$ phase of iron germanide, with a composition of 32 at.% Fe and 68 at.% Ge in the seed particle. Magnetite nanoparticles are possibly reduced to metallic Fe under the H_2 atmosphere[49] and then transformed into $FeGe_2$ with Ge uptake from the source. Otherwise, depending on the reaction kinetics and thermodynamics, $FeGe_2$ formation from Fe_3O_4 nanoparticle seed could be driven by the solid state reaction where germanium is incorporated into the lattice through a replacement mechanism.[49] Although either or both the scenarios could exist at our synthesis temperature, observation of the $FeGe_2$ phase at the tips of nanowires in the absence of a reduced atmosphere (with only Ar as carrier gas), confirms solid state replacement reaction of Fe_3O_4 as predominant process for germanide formation in our nanowire growth reaction. The elemental compositions of the metallic seeds were also confirmed from EDX mapping, where the distribution of Fe and Ge is shown in panel (b) of Figure 3. The elemental maps show a

homogeneous distribution of Fe and Ge in the seed particle, without much segregation or diffusion of Fe into the nanowire body. A TEM image (Figure 3(c)) of a <111> directed (SAED pattern in the inset confirms the growth direction) Ge nanowire, grown from a nanoparticle seed with a mean diameter of 21.5 nm, with a germanide metallic tip and the FFT pattern (inset of Figure 3(c)) obtained from a nanowire tip also confirms the presence of tetragonal $FeGe_2$, with a lattice spacing of 0.23 nm (theoretical lattice spacing of {211} plane of $FeGe_2$ is 0.232 nm (JCPDS cards #75-0033)). The heterogeneous interface; *i.e.* the non-planar contact line between the $FeGe_2$ seed and the Ge nanowire with two side facets at the catalyst-nanowire contact line, as shown in Figure 3(c), could result from compensation of the strain generated at the interface due to the large lattice mismatch between tetragonal $FeGe_2$ and diamond cubic Ge. The lattice mismatch between the tetragonal $FeGe_2$ seed crystal and the [111] Ge nanowire lattice is relaxed through the formation of {211} side facets at the seed-nanowire interface. The misfit and strain between seven {111} planes of Ge and ten {211} planes of $FeGe_2$ (seen at the seed-nanowire truncated facets in Figure 3(c)) is relaxed through the heterogeneous interface formation. Lattice spacing of cubic Ge {211} facets (JCPDS cards #04-0545) and tetragonal $FeGe_2$ {211} (JCPDS cards #75-0033) facets are close thus provides quasi-epitaxial matching at the interface. The lattice mismatch at the seed-nanowire interface can also be relaxed through the tilting of the seed at the tip of the nanowire. A reduction in the unit cell volume of tetragonal $FeGe_2$ (~0.173 nm^3) from the initial cubic Fe_3O_4 seed (~ 0.584 nm^3) is responsible for minimal expansion of the catalytic seeds during Ge nanowire growth, thus leading to nanowires with similar diameters to the growth particles.

In VSS-type growth, a precursor diffuses on the surface of a metal catalyst where it thermally decomposes to yield reactive Ge, which subsequently diffuses into the bulk metal

forming stable germanide compounds. The continued flux of the precursor increases the Ge content in the seeds, leading to nucleation of pure Ge crystals from $FeGe_2$, and the sustained growth of one-dimensional Ge single crystals. Using Fe_3O_4 as a promoter for Ge nanowire growth is preferable to pure transition metals, such as Fe or Ni, as unlike these cubic metals Fe_3O_4 will not undergo a large lattice expansion during the germination process. Hence, small diameter nanowires, with dimensions close to those of the starting catalyst are obtainable. For example, without taking account the surface diffusion and aggregation of nanoparticles during high temperature growth, Fe nanoparticles with a diameter of 14 nm will expand to $FeGe_2$ seeds of approximately 100 nm in diameter, due to lattice swelling (600-700 % lattice expansion is expected with germination). In calculating the size expansion of nanoparticles upon germanide formation we have used the unit cell volume expansion of Fe (PDF reference no. 06-0696) to FeGe (PDF reference no. 25-0357).

Compared to prototypical Au-Ge VLS growth, the binary Fe–Ge phase equilibrium (Figure S3 in Supporting Information) is more complex than the Au-Ge phase diagram and introduces a number of different germanide phases.[50] In the case of Fe, the Fe-Ge eutectic temperatures are significantly higher than the growth temperature used in this study and these systems form metal germanide compounds during growth. Since nanowire growth is performed at sub-eutectic temperatures, nucleation and growth of nanowires can be understood in the context of thermodynamic and kinetic factors governing the formation of germanide compounds. For three phase growth systems, VSS in this case as the eutectic temperature of the lowest Fe-Ge eutectic is significantly higher (850 °C) than the growth temperature, the seed particles will be saturated with the growth species, and the most favored thermodynamic phase will form depending on the experimental conditions, which under our conditions is the $FeGe_2$ alloy. To understand which phase forms first,

thermodynamic and kinetic aspects need to be considered. The '*first-phase rule*'[51] which was derived for silicide formation, but is also valid for germanide formation[52], states that "*the first crystalline phase nucleated will be the congruently melting compound next to the lowest temperature eutectic on the bulk equilibrium phase diagram*." The first-phase rule successfully predicts the phases formed in planar geometries, but does not reliably predict the phases observed in silicide nanowire growth.[53] In the case of Fe and Ge, the predicted phase according to the "first phase rule", and the experimentally observed phase, is tetragonal $FeGe_2$. The phase observed at the metal tip of the nanowire relates to the growth temperature, kinetic limitation of the germanide phase formation and the formation of coherent and semi-coherent interfaces to the nanowire surface.[14] During nanowire growth, the Ge species can either diffuse through the seed or migrate onto the surface of the particle-substrate interface, where the particle usually exhibits the highest degree of curvature. At the pinned catalyst-substrate interface, due to clustering of Ge adatoms through bulk and surface diffusion, preferred nucleation sites are created.[54] Both scenarios (bulk and surface diffusion) probably co-exist, however the bulk diffusion of Ge through the particles is probably a major contribution during the nanowire growth process, as confirmed by the existence of the Ge/Fe alloying process forming a germanide.

To further confirm the precise control of Ge nanowire diameters from Fe_3O_4 nanoparticle seeds, nanowires were also synthesized from magnetite nanoparticles with mean diameters of 7.2 (±1.5) and 21.5 (±3.2) nm. Ge nanowires with mean diameters of 12.5 (±4.2) nm and 19.5 (±5.2) nm were grown from the 7.2 and 21.5 nm magnetite seeds, respectively (Figure 4 (a) and (c)), as determined by TEM analysis (> 250 nanowires for each seed sample were investigated). A depression of the melting point and the Tamman temperature, *i.e.* the temperature required to initiate the surface diffusion of nanoparticles, typically half of

melting point temperature, was expected for the smallest nanoparticles with a mean diameter of 7.2 nm (bulk melting point of Fe_3O_4 is 1600 ºC). Thus, at our growth temperature (460 ºC), for the lowest sized nanoparticles, using a nanoparticle concentration (90 μmole cm^{-3}) similar to that used for the larger diameter nanoparticles (14 and 21.5 nm), yielded much larger diameter nanowires compared to the nanoparticle size. To address this issue, nanowire growth experiments were performed from Fe_3O_4 catalysts by reducing the density of the catalyst nanoparticles by half (45 μmole cm^{-3}). This reduction of nanoparticle concentration resulted in the growth of nanowires with an almost similar diameter range (8.8 (± 3.5) nm) to the initial nanoparticle seeds, with a reduction of nanowire yield at same temperature, thus confirming the radial control over the nanowire diameters against Fe_3O_4 seeds in sub-10 nm regime.

Polytype and Twin formation in Nanowires: A twin boundary is isolated to a single atomic plane that separates two neighbouring crystal domains, with very specific relative crystallographic orientations and without any dangling bonds at their interface. In this study, a number of nanowires (2-4 %) with lateral twin boundaries, grown from colloidal spherical Fe_3O_4 seeds with mean diameters of 14 and 21.5 nm, were observed. To further investigate the formation and arrangements of twin planes in <111>-oriented Ge nanowires, hemispherical shaped Fe_3O_4 nanodots of around 20 nm diameter were fabricated through block co-polymer (BCP) lithography (detailed synthesis process given in Supporting Information) on Si (001) substrates with a native surface oxide (Figure 5(a) and S4 in Supporting Information).[55] These particular magnetite nanodot catalysts are suitable (due to the particular curvature of the catalyst-substrate and catalyst-nanowire interface and adherence of the BCP patterned nanodots with substrate) to promote the growth of large numbers of <111> oriented Ge nanowires with lateral growth of twin planes perpendicular to

the nanowire growth axis (15-20 %, based on studying 250 nanowires per sample). The radial dimensions of nanowires grown from BCP patterned magnetite catalysts (20.8 (± 5.2) nm, see Figure S5 in Supporting Information) matched well with the radial dimension of the nanodots prior to nanowire growth (mean diameter ~ 21 nm). The lengths of the Ge nanowires synthesized were between 2 to 5 microns (Figure 5 (b)). Bright-field TEM analysis of a multi-twinned Ge nanowire is depicted in Figure 5 (More examples of twinned nanowires are shown in Figure S6), which highlights the dense contrast pattern along the length of a <111>-oriented nanowire due to the formation of multiple planar defects on (111) planes perpendicular to nanowire growth axis (Figure 5(c), (d) and S6). These planar defects observed throughout the entire nanowire length, indicate a continuous inherent influence, rather than a sudden fluctuation in growth conditions, behind the formation of the defective structures. The detailed structural nature of the differently contrasted domains (dark and bright) were analysed through HRTEM. Single crystalline 3C-diamond cubic regions of lengths between 5-15 nm (Figure 5 (d)) and with *abcabc* stacking were observed between faulty twin planes (Figure 5 (e)). A 60° rotation of crystal orientation on both sides (A and B) of the twin planes with the growth axis represents a mirror reflection of a 3C stacking order of the {111} planes without any bond-breakage at the interface. The TEM image shown in Figure 5(e) is viewed along the <110> zone axis. Periodic modulations of altering (-1-11) and (-1-1-1) 3C cubic lateral facets, making an angle of ~ 141º were observed when viewed along the <110> zone axis, which is similar to the observation of twins in zinc-blende InAs nanowire segments[36] or Cu-seeded twinned Si nanowires[39] . The inset of Figure 5(e) shows the FFT pattern (in the inset of the figure) from the TEM image of the two diamond cubic segments (A and B) separated by two single twin planes (circled in the image); the double spot pattern is associated with twin formation. The FFT depicts the same growth axis [1-11] for both the cubic segments (shown in FFT with C(1-11) indexing) on either side of

the twin plane. The nanofaceted morphology of the grown nanowires could make them ideal candidates for thermoelectric applications, due to predicted low thermal conductivity compared to their smooth faceted counterpart.[29]

For Si and Ge, non-lamellar twin boundaries have previously been observed in <112> directed nanowires.[16, 38, 56] Using classical nucleation theory, Johansson *et al.* have proposed[57] that the energy barrier (ΔG_T) for the nucleation of a semi-circular twin nucleus, of radius *r* and height *h*, at the triple phase boundary (TPB), depends on the sum of the nucleus energy of a {111} plane, the twinning energy and the energy of the surface step associated with the nucleus: $\Delta G_T = -\frac{\pi}{2} r^2 \left(\frac{\Delta\mu}{S} - \gamma_t\right) + (\pi\sigma_{ls} + 2\sigma_{sv}) rh$, where *S* is the inverse of the nucleation site density on a {111} plane, $\Delta\mu$ is the chemical potential, γ_t is the twin energy and all the σ_s terms are different interfacial energies. As the twin energy (γ_t) is small compared to the $\Delta\mu/S$, the energy barrier does not change significantly for a twinned or ordinary nucleation. Controlled manipulation of the thermodynamics and interfacial surface chemistries at the nanoscale is required for 'forced' twin plane nucleation. Random twinning in the semiconductor nanowires can be interpreted from fluctuations in mass-transport to the TPB. This idea was refined by considering the interfacial tensions at the TPB and the deformation of the catalyst particle during crystal growth.[37] The growth of <111> twinned nanowires takes place differently because the angle formed by {111} micro(nano) facets with respect to the TPB is either acute (v = 71°) or obtuse (v = 109°). This effect causes the droplet to deform asymmetrically and the wetting angle to change, which governs the process of twin nucleation. Hence, the fluctuation in the contact angle between the seed and the nanowire must be large enough to accommodate surface "refaceting" without hindering nanowire growth. Au-seeded growth of Si or Ge nanowires does not permit the formation of periodic twins in <111> directed nanowires because of the small wetting angle variation.

Whereas for Fe_3O_4 seeded Ge nanowire growth, heteroepitaxy and strain at the catalyst-nanowire interface is more likely to trigger twin boundary nucleation.

The role of hemispherical shaped magnetite nanodots (mean diameter ~ 21 nm) for the growth of Ge nanowires with lateral twin boundaries is highlighted by the fact that hematite Fe_2O_3 nanoparticles, metallic Fe nanoparticles and spherical Fe_3O_4 nanoparticles of similar dimensions did not yield many twinned <111> Ge nanowires. In fact, under our reaction conditions no <111> twinned Ge nanowires were formed with hematite Fe_2O_3 or metallic Fe nanoparticle seeds and for spherical magnetite nanoparticles the yield was much lower than BCP patterned hemispherical nanodot catalysts (3-4% compared to 15-20% with hemispherical nanodots). Nanowire growth is a layer-by-layer process with single nucleation events at the catalyst-nanowire interface. Orientation of critical nuclei at the interface determines the formation of twin or normal plane crystals because the difference in the energy barrier for twin and normal plane nucleation is very small. The presence of both Fe^{2+} and Fe^{3+} ions in the Fe_3O_4 nanodots (see X-ray photoelectron spectroscopic (XPS) analysis of nanodots in Figure S4 showing the presence of both of the ions) can induce competitive kinetics in the germination process during nanowire growth, thus generating enormous strain at the catalyst-substrate and catalyst-nanowire interface. For spherical nanoparticle seeds (either in solution or on the substrate), this strain can be relaxed through shape deformation, rotation or preferred nucleation at a suitable curvature. However, for the hemispherical BCP-patterned nanodot seeds attached to the substrate, competitive germination processes with the nanodots can results in a stretching and narrowing of the hemispherical seed-substrate and seed-nanowire interface, thus triggering the formation of nanofaceted side-walls[58] and lateral twin boundaries at the seed-nanowire interface (Figure S7). The highly weighted curvature at the corner of the hemispherical seed-nanowire interface, the shape-stability of the nanodots

and competitive germination processes within the magnetite catalysts together evoke faulted nucleation at the corner facets and lateral propagation of twin boundaries. A pseudoepitaxial relationship between the complex alloy catalyst and the germanium nanowires can influence a layer-by-layer arrangement in the triple phase interface to promote lateral stacking fault. Previously, the growth of lateral {111} twins in <111>-oriented Si nanowires were assigned to the role of Cu as a solid-state catalyst in nanowire growth.[39] However, as lateral twin structures are not frequently observed in group IV nanowires seeded from solid sub-eutectic catalysts, we can conclude that other growth parameters such as, peculiarities in the shape of a catalyst, the rate of germination *etc*., plays an important role in twin plane growth. Detailed in-situ growth inside a TEM is needed to deduce the growth mechanism of lateral twin boundaries in Ge nanowires.

Controlling the density of twin planes in the nanowire could be useful for fundamental electron and phonon transport properties. In our case, a clear dependence of the periodicity of coherent twin planes on the diameter of Ge nanowires, grown with 21 nm diameter BCP patterned nanodots was observed. Figure 6(a) shows the relationship between the twin plane density, *i.e.* the number of lateral twin planes in a certain nanowire length (for twin density calculation we estimated twin planes in 500 nm lengthscale of nanowires), as a function of the measured nanowire diameter. Twin densities increase with increasing nanowire diameter up to a measured diameter of ~ 50 nm. The density of twin boundaries along the entire length of a nanowire (on five or more nanowires with the same diameter) was determined by TEM. Insets in Figure 6(a) show two representative nanowires of different diameters (d = 15 and 30 nm) with different densities of twin planes. Thinner nanowires, due to their large surface areas can compensate the strain at the seed-nanowire interface through sidewall

relaxation, whereas for large diameter nanowires strain at the catalyst-nanowire interface can trigger the formation of dense stacking faults in the {111} plane.

Periodic twinned planes can generate polytype superstructures where stacking faults in the *abc* stacking sequence along the <111> direction can produce local hexagonal ordering in a cubic crystal, for example, *aba*, leading to polytypes with distinctly unique properties. The polytype combination of lonsdaleite (2H)/diamond (3C) leads to a type-I heterostructure, where both electrons and holes are localized in the region of the hexagonal polytype.[59] These novel structures can act as crystal phase quantum dots in a chemically homogeneous nanowire.[33] In the densely faulted regions of a nanowire, *i.e.* in nanowires with a high twin density, successive {111} stacking faults result in a change in the stacking sequence from 3C to other polymorphs. In the present case, mainly for relatively large nanowires (> 20 nm), cubic 3C stacking in tetrahedral coordination in the <111> direction changed locally to 4H polytypes (Figure 6(b) and S8). Local diversion of *abcabc* stacking of close-packed atomic arrangement in a (111) plane in a diamond-type cubic structure (Ge-I) in Ge nanowires locally changes to an $a^{''}b^{''}c^{''}b^{''}a^{''}b^{''}c^{''}b^{''}$ arrangement of the 4H-Ge polytype with a 50 % hexagonal layer. Diamond α-Ge is an indirect bandgap semiconductor with a band gap of 0.66 eV, whereas the nature of the 4H-Ge as semiconductor is contradictory. In one case, based on DFT-LDA calculation 4H-Ge was predicted to be a zero band gap semiconductor with slight metallic character.[60] However a recent finding through B3LYP calculations suggests a direct band gap of 0.81 eV located at Γ point for 4H-Ge while the same calculation yields a band gap of α-Ge as 0.83 eV.[61] In both scenarios, hexagonal 4H-Ge region can form a region up to few nanometers with altered band structure in a 3C-Ge nanowire host lattice.

To confirm the presence of polytypes in Ge nanowires we have performed Raman spectroscopy measurements on single nanowires by dispersing them on TEM grids and correlating the results with TEM observations. The measurements were performed on a LabRam HR (Jobin Yvon) spectrometer equipped with a 600 gr/mm grating, an edge filter and a CCD detector. A diode laser of wavelength 785 nm was used as an excitation source and a 100× objective with a numerical aperture (NA) of 0.9 was used to get the laser spot diameter of ~2 μm. The Raman spectra of normal (non-defective) and defective nanowires are displayed in Figure 6(c). A TEM image of the corresponding polytype nanowire is shown in Figure 6(b). For reference we have also presented Raman spectrum of bulk Ge. Spectra were fitted using Lorentzian functions. All the spectra exhibit a Raman peak corresponding to the Ge-Ge vibrational mode. In the defected nanowire another peak was observed at 284 cm^{-1} in addition to Ge-Ge mode. For a normal 3C nanowire (diameters ~ 30 nm grown with Fe_3O_4 nanodots) the Ge-Ge vibrational mode appeared at 294 cm^{-1}, which is shifted towards a lower wavenumber with respect to the same mode of bulk Ge. In the defect free pure 3C nanowires the single peak observed is due to a triply degenerated E_{2g} mode from a diamond cubic structure.[62] The red shift is due to the combined effects of phonon confinement and laser induced heating. On the other hand, in a twinned nanowire of similar diameter (Figure 6(b)) the Ge-Ge mode appeared at 296 cm^{-1}. The presence of polytype structures in the defected nanowires introduces strain which shifts the Ge-Ge mode towards higher a wavenumber (by 2 cm^{-1}). Therefore, the lower red shift in twinned (4 cm^{-1}) compared to normal nanowires (6 cm^{-1}) is due to a strain-induced blue shift introduced by the polytype structures.[63] Only a Ge-Ge Raman mode was observed for the normal nanowires, whereas an additional Raman peak situated at 284 cm^{-1} was detected for the twinned nanowires. This new peak arises due to the deviation from the 3C stacking sequence and the presence of 4H Ge in the nanowires, where the stacking fault modifies the Raman polarizability tensors. The

vibrational modes of 4H Ge can be obtained by folding the Brillouin zone of a diamond lattice.[64] The observed peak at 284 cm^{-1} is due to the presence of 4H Ge, as confirmed from TEM analysis of corresponding Ge nanowires (Figure 6(b)) and is consistent with the earlier reports.[61] We did not observe any other polytype sequences such as 2H or 9R (Ramsdell classification scheme) by HRTEM analysis. Also, the presence of other polytypes would create zone folding of phonon dispersion, resulting new optical phonon branches and new Raman modes. The frequency and relative intensities of the folded modes are typical characteristic of the stacking sequence of each polytype. Only the Raman signal for the 4H stacking sequence was observed from the faulted Ge nanowires.

Conclusions

In summary, we have demonstrated the size selective growth of Ge nanowires, even in the sub-10 nm regime, by solid phase seeding using magnetite nanocrystals as catalysts. Highly crystalline nanowires predominantly grew along the <110> direction, with some of the <111>-directed nanowires demonstrating lateral {111} twins. The magnificent size retention of the magnetite iron oxide catalysts (and possibly other metal oxides) make them feasible alternatives to sub-eutectic metal catalysts such as Fe, Ni, Cu *etc*. for VSS-type nanowire growth. Apart from the superior size retention, BCP patterned magnetite nanodots triggered the growth of coherent twin boundaries perpendicular to the <111>-oriented nanowire growth axis. The sequential occurrence of twin planes resulted in a localized hexagonal region in the diamond cubic nanowires, with the prospect of having a quantum well structure from a homogeneous single group IV nanowire. Ultimately controlling the position of twin planes could lead towards the formation of twinning superlattices or a polytypic superlattices in elemental group IV nanowire systems with a range of new physical properties.

Acknowledgements

We acknowledge financial support from Science Foundation Ireland (SFI Grant: 09/IN.1/I2602) and SFI International Strategic Co-operation Award (ISCA) India-Ireland program.

Supporting Information Description

Nanowire and seed nanoparticle synthesis, BCP lithography process to fabricate Fe_3O_4 nanodot arrays, nanowires including twin boundaries, Fe-Ge phase diagram, TEM images with catalyst tips and polytype formation are shown in Supporting Information. This material is available free of charge via the internet at http://pubs.acs.org

References:

1. Burchhart, T.; Zeiner, C.; Lugstein, A.; Henkel, C.;Bertagnolli, E. *Nanotechnology* **2011,** *22*, 035201.
2. Garnett, E.;Yang, P. D. *Nano Lett.* **2010,** *10*, 1082-1087.
3. He, R. R.; Gao, D.; Fan, R.; Hochbaum, A. I.; Carraro, C.; Maboudian, R.;Yang, P. D. *Advanced Materials* **2005,** *17*, 2098-+.
4. Liu, Y.-C. C.; Rieben, N.; Iversen, L.; Sorensen, B. S.; Park, J.; Nygard, J.;Martinez, K. L. *Nanotechnology* **2010,** *21*.
5. Seo, M. H.; Park, M.; Lee, K. T.; Kim, K.; Kim, J.;Cho, J. *Energy Environ. Sci.* **2011,** *4*, 425-428.
6. Wu, X. Y.; Kulkarni, J. S.; Collins, G.; Petkov, N.; Almecija, D.; Boland, J. J.; Erts, D.;Holmes, J. D. *Chem. Mat.* **2008,** *20*, 5954-5967.
7. Xiang, J.; Lu, W.; Hu, Y. J.; Wu, Y.; Yan, H.;Lieber, C. M. *Nature* **2006,** *441*, 489-493.
8. Dasgupta, N. P.; Sun, J.; Liu, C.; Brittman, S.; Andrews, S. C.; Lim, J.; Gao, H.; Yan, R.;Yang, P. *Advanced Materials* **2014,** *26*, 2137-2184.
9. Leonard, F.; Talin, A. A.; Swartzentruber, B. S.;Picraux, S. T. *Physical review letters* **2009,** *102*, 106805.
10. O'Regan, C.; Biswas, S.; O'Kelly, C.; Jung, S. J.; Boland, J. J.; Petkov, N.;Holmes, J. D. *Chem. Mat.* **2013,** *25*, 3096-3104.
11. Rathi, S. J.; Smith, D. J.;Drucker, J. *Nano Lett.* **2013,** *13*, 3878-3883.
12. Wang, H.; Zepeda-Ruiz, L. A.; Gilmer, G. H.;Upmanyu, M. *Nature communications* **2013,** *4*, 1956-1956.
13. Richards, B. T.; Gaskey, B.; Levin, B. D. A.; Whitham, K.; Muller, D.;Hanrath, T. *Journal of Materials Chemistry C* **2014,** *2*, 1869-1878.
14. Lensch-Falk, J. L.; Hemesath, E. R.; Perea, D. E.;Lauhon, L. J. *J. Mater. Chem.* **2009,** *19*, 849-857.
15. Geaney, H.; Mullane, E.;Ryan, K. M. *Journal of Materials Chemistry C* **2013,** *1*, 4996-5007.
16. Biswas, S.; Singha, A.; Morris, M. A.;Holmes, J. D. *Nano Lett.* **2012,** *12*, 5654-5663.
17. Hanrath, T.;Korgel, B. A. *Advanced Materials* **2003,** *15*, 437-440.
18. Biswas, S.; O'Regan, C.; Petkov, N.; Morris, M. A.;Holmes, J. D. *Nano Lett.* **2013,** *13*, 4044-4052.
19. Park, W. I.; Zheng, G.; Jiang, X.; Tian, B.;Lieber, C. M. *Nano Lett.* **2008,** *8*, 3004-3009.
20. Barth, S.; Kolesnik, M. M.; Donegan, K.; Krstic, V.;Holmes, J. D. *Chem. Mat.* **2011,** *23*, 3335-3340.
21. Schmidt, V.; Senz, S.;Gosele, U. *Nano Lett.* **2005,** *5*, 931-935.
22. Qi, W. H.;Wang, M. P. *Materials Chemistry and Physics* **2004,** *88*, 280-284.
23. Petkov, N.; Birjukovs, P.; Phelan, R.; Morris, M. A.; Erts, D.;Holmes, J. D. *Chem. Mat.* **2008,** *20*, 1902-1908.
24. Lotty, O.; Biswas, S.; Ghoshal, T.; Glynn, C.; O'Dwyer, C.; Petkov, N.; Morris, M. A.;Holmes, J. D. *Journal of Materials Chemistry C* **2013,** *1*, 4450-4456.
25. Cao, G.;Liu, D. *Advances in Colloid and Interface Science* **2008,** *136*, 45-64.
26. Tuan, H. Y.; Lee, D. C.; Hanrath, T.;Korgel, B. A. *Chem. Mat.* **2005,** *17*, 5705-5711.
27. Wood, E. L.;Sansoz, F. *Nanoscale* **2012,** *4*, 5268-5276.
28. Tsuzuki, H.; Cesar, D. F.; de Sousa Dias, M. R.; Castelano, L. K.; Lopez-Richard, V.; Rino, J. P.;Marques, G. E. *ACS Nano* **2011,** *5*, 5519-5525.
29. Sansoz, F. *Nano Lett.* **2011,** *11*, 5378-5382.
30. Akiyama, T.; Yamashita, T.; Nakamura, K.;Ito, T. *Nano Lett.* **2010,** *10*, 4614-4618.
31. Ikonic, Z.; Srivastava, G. P.;Inkson, J. C. *Physical Review B* **1995,** *52*, 14078-14085.
32. Ikonic, Z.; Srivastava, G. P.;Inkson, J. C. *Surface Science* **1994,** *307*, 880-884.
33. Akopian, N.; Patriarche, G.; Liu, L.; Harmand, J. C.;Zwiller, V. *Nano Lett.* **2010,** *10*, 1198-1201.
34. Nakamura, J.;Natori, A. *Applied Physics Letters* **2006,** *89*.

35. Algra, R. E.; Verheijen, M. A.; Borgstrom, M. T.; Feiner, L.-F.; Immink, G.; van Enckevort, W. J. P.; Vlieg, E.;Bakkers, E. P. A. M. *Nature* **2008,** *456*, 369-372.
36. Caroff, P.; Dick, K. A.; Johansson, J.; Messing, M. E.; Deppert, K.;Samuelson, L. *Nature Nanotechnology* **2009,** *4*, 50-55.
37. Davidson, F. M.; Lee, D. C., III; Fanfair, D. D.;Korgel, B. A. *Journal of Physical Chemistry C* **2007,** *111*, 2929-2935.
38. Lopez, F. J.; Hemesath, E. R.;Lauhon, L. J. *Nano Lett.* **2009,** *9*, 2774-2779.
39. Arbiol, J.; Fontcuberta i Morral, A.; Estrade, S.; Peiro, F.; Kalache, B.; Roca i Cabarrocas, P.;Ramon Morante, J. *Journal of Applied Physics* **2008,** *104*.
40. Shin, N.; Chi, M.; Howe, J. Y.;Filler, M. A. *Nano Lett.* **2013,** *13*, 1928-1933.
41. Fontcuberta i Morral, A.; Arbiol, J.; Prades, J. D.; Cirera, A.;Morante, J. R. *Advanced Materials* **2007,** *19*, 1347-+.
42. Vincent, L.; Patriarche, G.; Hallais, G.; Renard, C.; Gardes, C.; Troadec, D.;Bouchier, D. *Nano Lett.* **2014,** *14*, 4828-4836.
43. Ikonic, Z.; Srivastava, G. P.;Inkson, J. C. *Physical Review B* **1995,** *52*, 1474-1476.
44. Park, J.; An, K. J.; Hwang, Y. S.; Park, J. G.; Noh, H. J.; Kim, J. Y.; Park, J. H.; Hwang, N. M.;Hyeon, T. *Nature Materials* **2004,** *3*, 891-895.
45. Yang, H.-J.;Tuan, H.-Y. *J. Mater. Chem.* **2012,** *22*, 2215-2225.
46. Wu, Y.; Cui, Y.; Huynh, L.; Barrelet, C. J.; Bell, D. C.;Lieber, C. M. *Nano Lett.* **2004,** *4*, 433-436.
47. Tuan, H.-Y.; Lee, D. C.;Korgel, B. A. *Angewandte Chemie-International Edition* **2006,** *45*, 5184-5187.
48. Lee, D. C.; Mikulec, F. V.;Korgel, B. A. *Journal of the American Chemical Society* **2004,** *126*, 4951-4957.
49. Olsen, A.;Sale, F. R. *Journal of Materials Science* **1978,** *13*, 2157-2163.
50. Massalaski, T. B. *Binary Alloy Phase Diagrams*. 2nd ed.; ASM International: 1990.
51. Walser, R. M.;Bene, R. W. *Applied Physics Letters* **1976,** *28*, 624-625.
52. Wittmer, M.; Nicolet, M. A.;Mayer, J. W. *Thin Solid Films* **1977,** *42*, 51-59.
53. Schmitt, A. L.; Higgins, J. M.; Szczech, J. R.;Jin, S. *J. Mater. Chem.* **2010,** *20*, 223-235.
54. Cheyssac, P.; Sacilotti, M.;Patriarche, G. *Journal of Applied Physics* **2006,** *100*.
55. Ghoshal, T.; Maity, T.; Godsell, J. F.; Roy, S.;Morris, M. A. *Advanced Materials* **2012,** *24*, 2390-2397.
56. Barth, S.; Boland, J. J.;Holmes, J. D. *Nano Lett.* **2011,** *11*, 1550-1555.
57. Johansson, J.; Karlsson, L. S.; Svensson, C. P. T.; Martensson, T.; Wacaser, B. A.; Deppert, K.; Samuelson, L.;Seifert, W. *Nature Materials* **2006,** *5*, 574-580.
58. Ross, F. M.; Tersoff, J.;Reuter, M. C. *Physical review letters* **2005,** *95*.
59. Fissel, A.; Bugiel, E.; Wang, C. R.;Osten, H. J. *Materials Science and Engineering B-Solid State Materials for Advanced Technology* **2006,** *134*, 138-141.
60. Raffy, C.; Furthmuller, J.;Bechstedt, F. *Physical Review B* **2002,** *66*.
61. Kiefer, F.; Hlukhyy, V.; Karttunen, A. J.; Faessler, T. F.; Gold, C.; Scheidt, E.-W.; Scherer, W.; Nylen, J.;Haeussermann, U. *J. Mater. Chem.* **2010,** *20*, 1780-1786.
62. Jeon, N.; Dayeh, S. A.;Lauhon, L. J. *Nano Lett.* **2013,** *13*, 3947-3952.
63. Dillen, D. C.; Varahramyan, K. M.; Corbet, C. M.;Tutuc, E. *Physical Review B* **2012,** *86*.
64. Lopezcruz, E.;Cardona, M. *Solid State Communications* **1983,** *45*, 787-789.

Figures

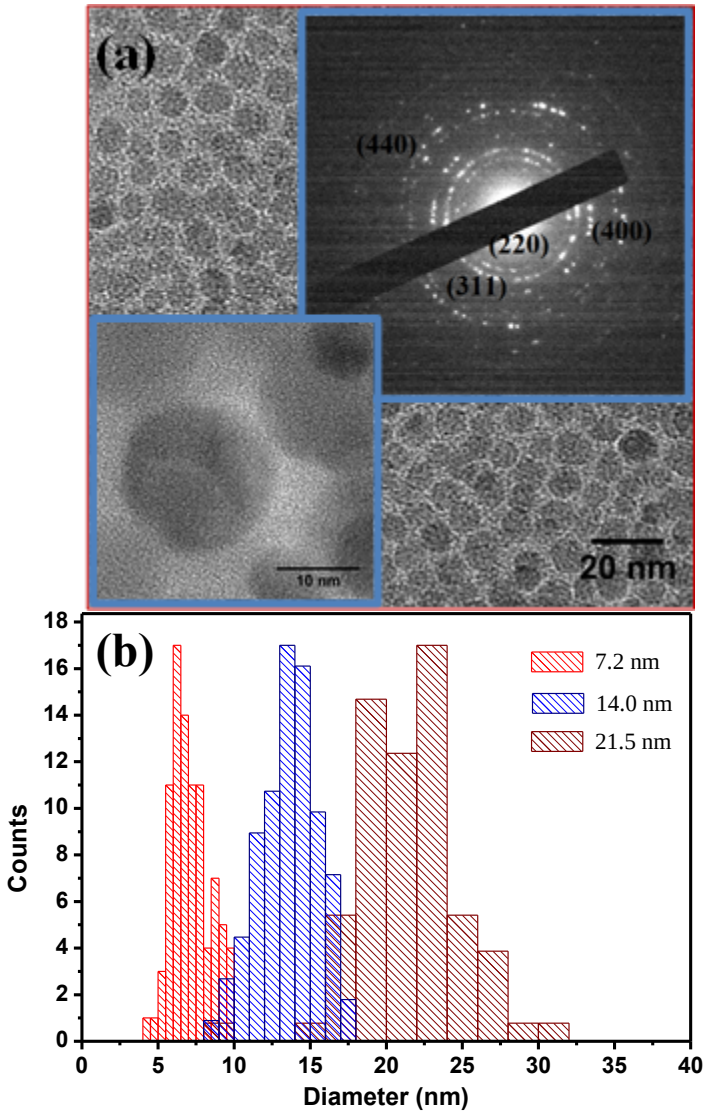


Figure. 1. (a) TEM image showing the smallest size colloidal Fe_3O_4 nanoparticles synthesized (~ 7 nm mean diameter). SAED in the inset confirms the formation of magnetite phase. (b) Diameter distributions for different Fe_3O_4 nanoparticle catalysts, revealing the mean diameter of nanoparticles to be 7, 14 and 21 nm.

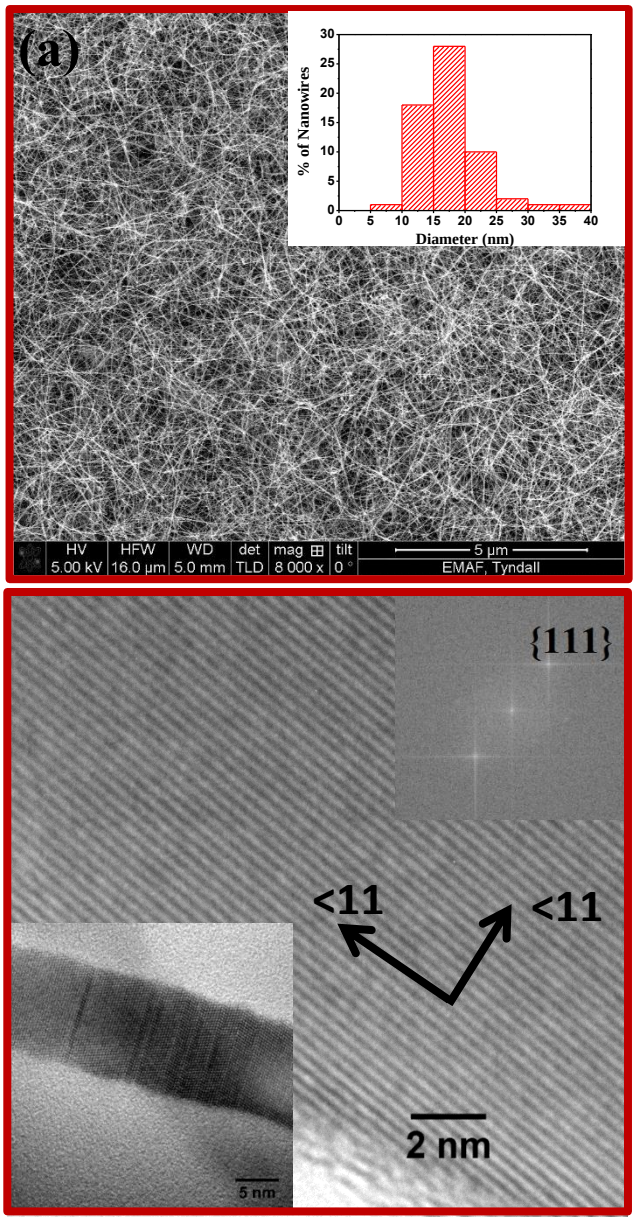


Figure. 2. (a) SEM image depicting the formation of a high density of Ge nanowires from Fe_3O_4 nanoparticle seeds. The inset shows diameter distribution uniformity of the nanowires produced. The HRTEM image shown in part (b) represents a highly crystalline nanowire with a <111> growth direction. Corresponding FFT in the inset shows the formation of highly crystalline diamond cubic Ge nanowires with <111> orientation. Another inset also shows a <111> directed Ge nanowire with {111} radial twinning.

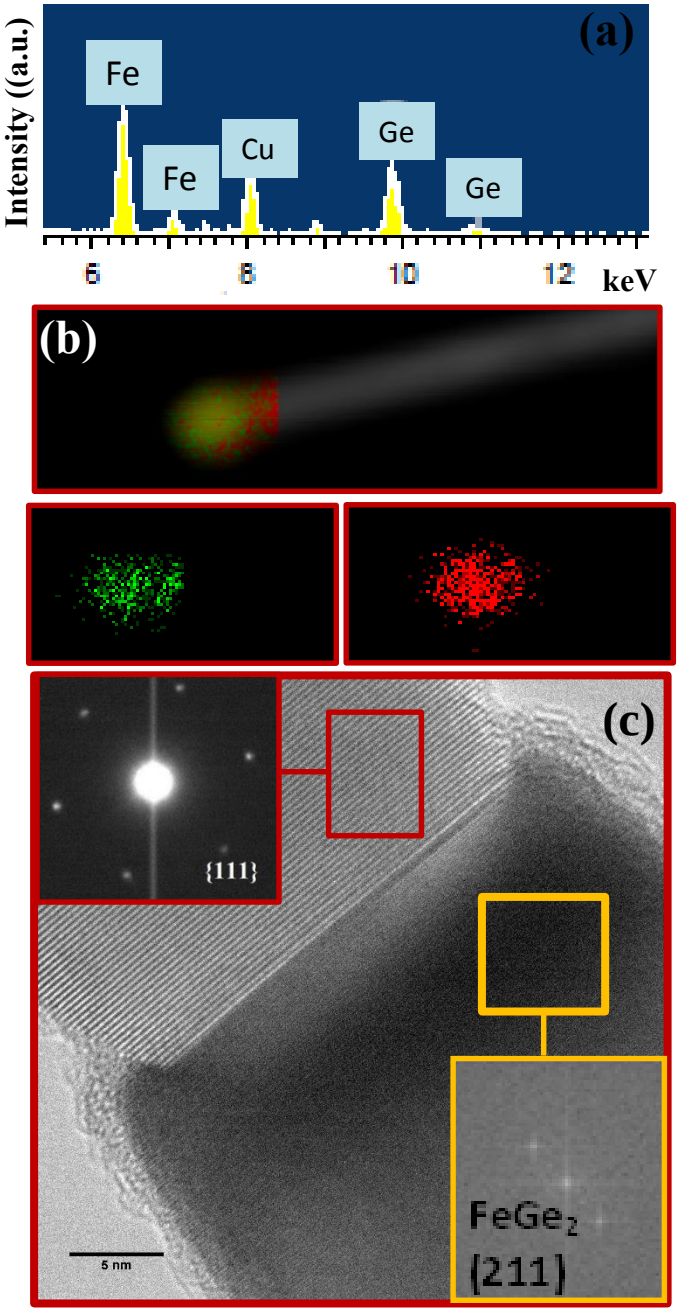


Figure. 3. (a) Point EDX spectrum recorded from the tip of the nanowire showing the presence of both Fe and Ge (Fe: 32 at.% and Ge: 68 at.%). (b) EDX mapping of a nanowire revealing Ge signal (red) from the body of the nanowire and Fe (green) and Ge from the tip. Part (c) represents TEM image of a <111> directed Ge nanowire with $FeGe_2$ tip. FFT in the inset correspond to the $FeGe_2$ phase at the tip and SAED in the inset matches with the diamond cubic crystal structure of Ge for the nanowire body.

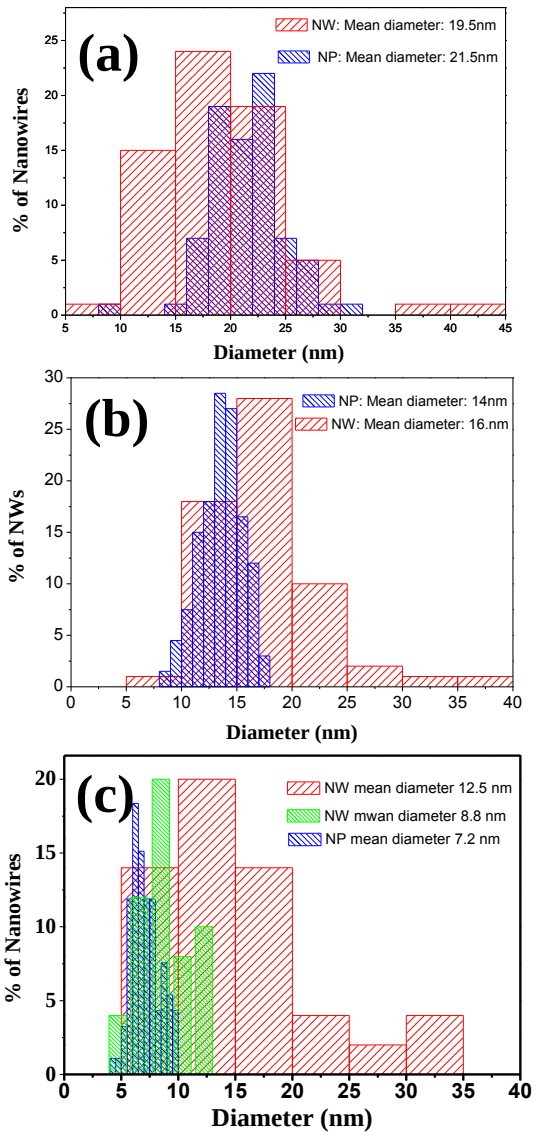


Figure 4. Diameter distributions for Ge nanowires grown from Fe_3O_4 nanoparticles with mean diameters of: (a) 21.5 nm, (b) 14 nm and (c) 7.2 nm. Diameter distribution (green distribution) in Part (c) reveals thinner nanowires upon lowering the nanoparticle (7 nm) concentration.

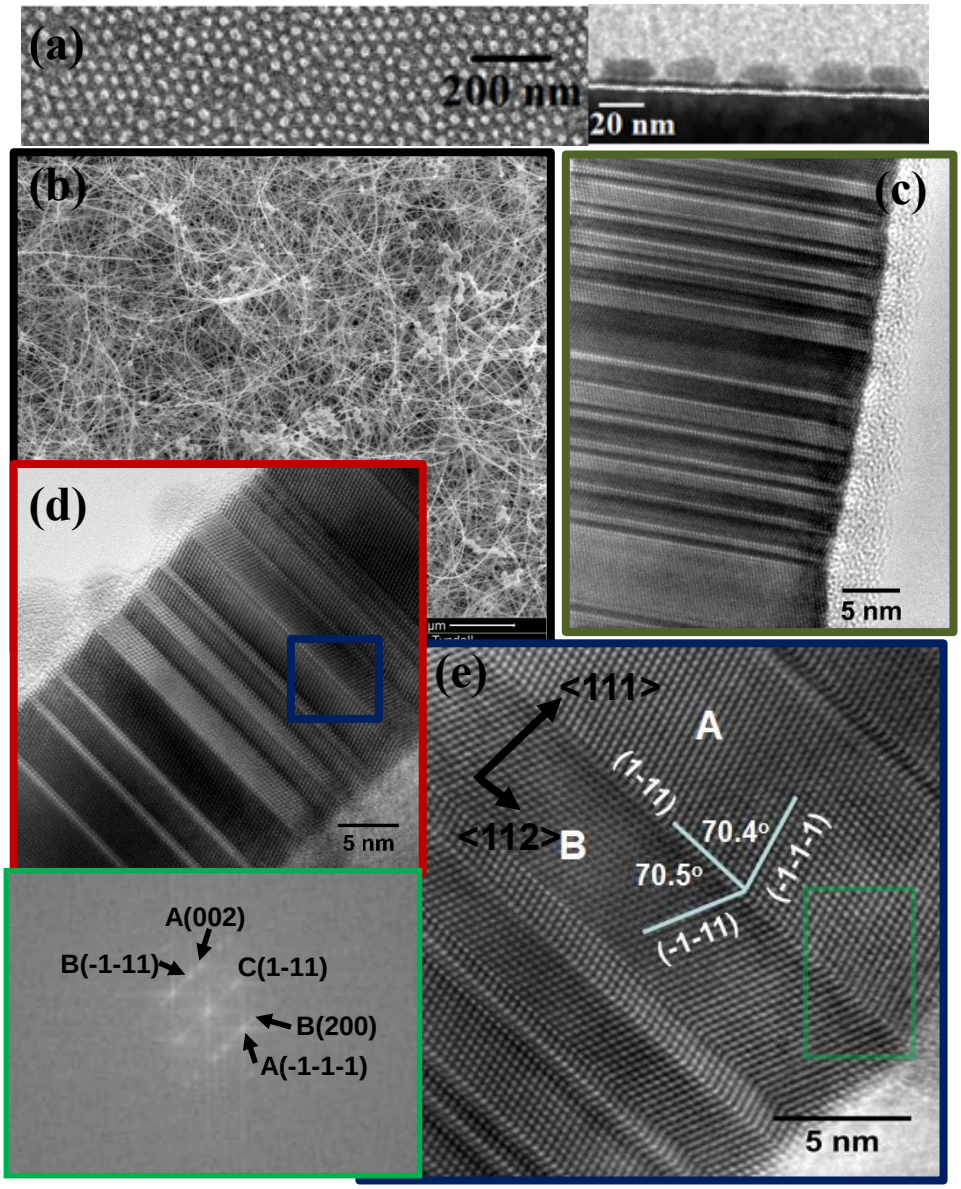


Figure 5. (a) SEM image and cross-sectional TEM image (inset) of BCP patterned Fe_3O_4 nanodots. (b) SEM image shows the growth of a high yield of Ge nanowires from BCP patterned nanodots. Parts (c) and (d) portray bright-filed TEM images with lateral twin boundaries perpendicular to the <111> nanowire growth axis. HRTEM image in part (e) shows the formation of {111} twin planes where two 3C mirror segments (A and B) are separated by twin boundaries (also shown in the FFT pattern in the inset). The angles between the nanofacets are measured to be ~ 141°. Corresponding FFT data obtained from the marked region shows a <111> growth orientation.

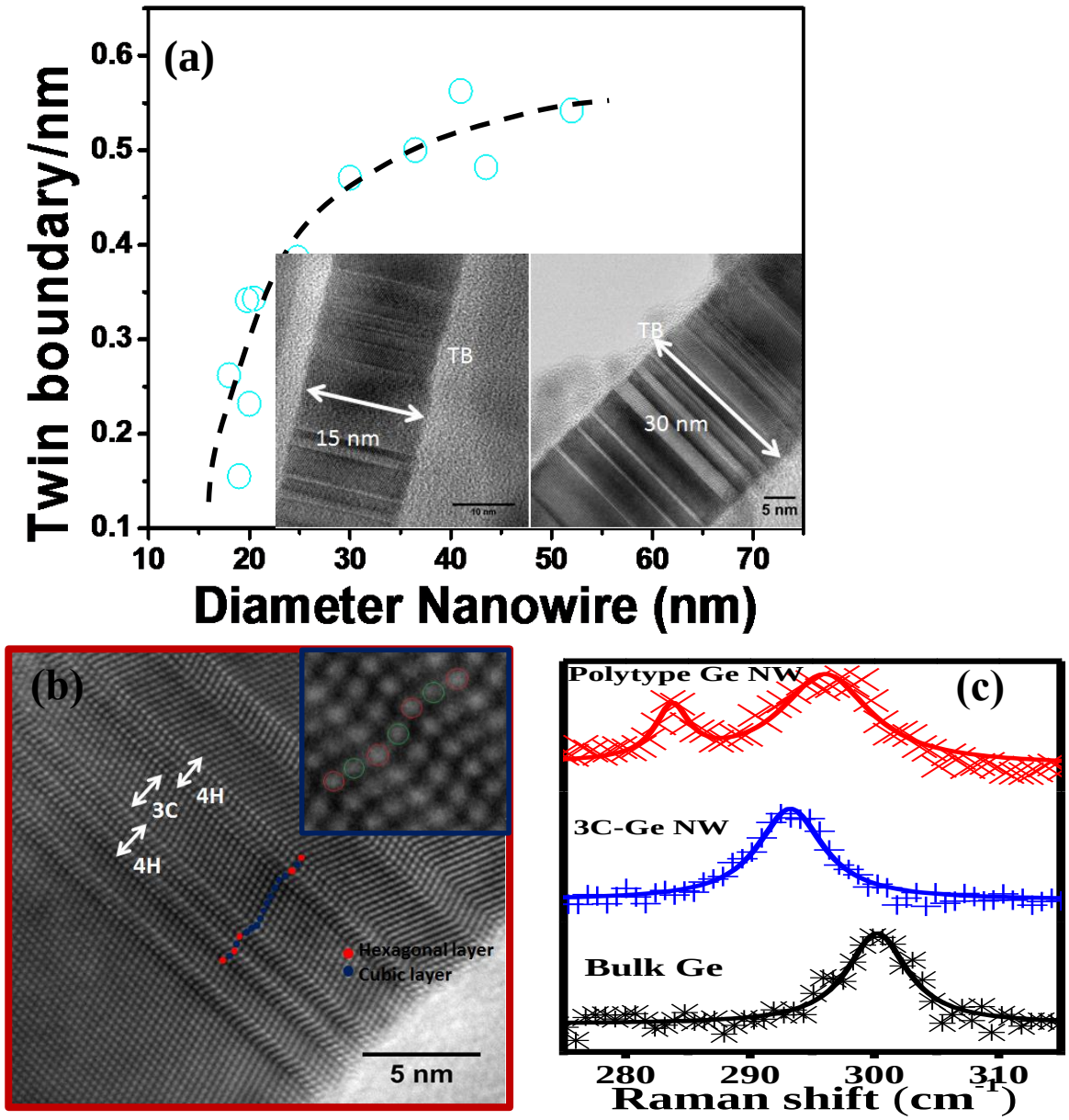
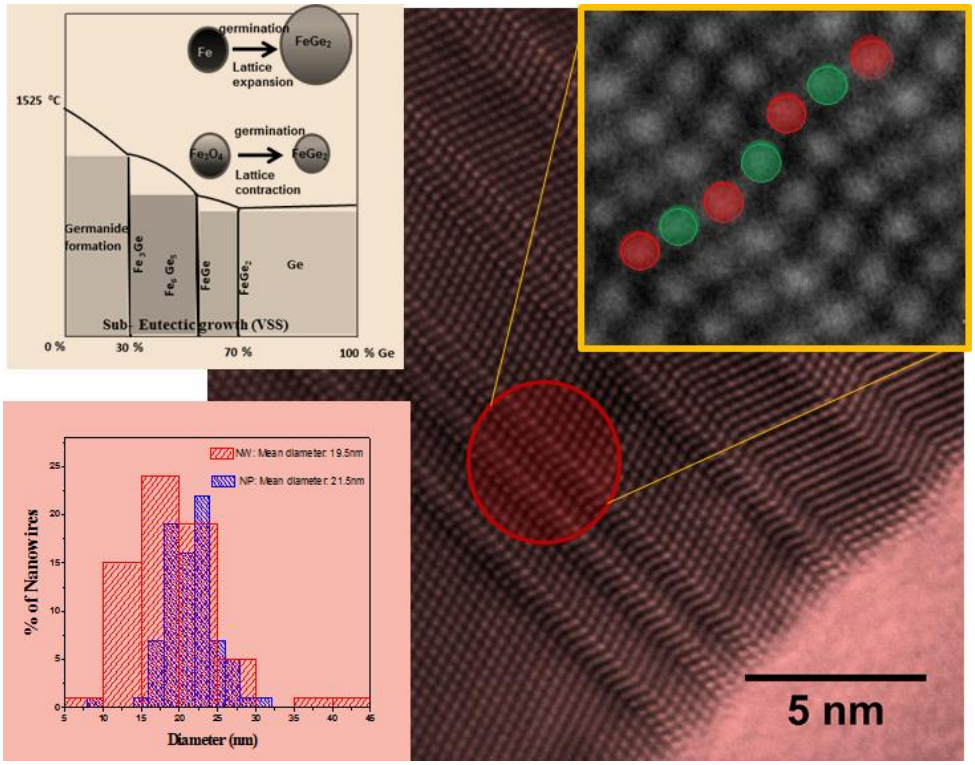


Figure 6. Plot in part (a) the change in the twin plane density as a function of nanowire diameter; the TEM images as insets represent two different diameter nanowires with dissimilar twin plane distribution. The HRTEM image shown in (b) and the inset portray the formation of a 4H-polytype in a 3C diamond cubic nanowire. Polytype regions are marked by color dots. (c) Raman spectra of 3C-Ge, polytype and bulk Ge nanowires with laser power density of 1 mW/ μm^2.

TOC graphic:


germination
Fe
FeGe2
Lattice expansion
1525 °C
germination
Fe3O4
FeGe2
Lattice contraction
Germanide formation
Fe3Ge
Fe6Ge5
FeGe
FeGe2
Ge
Sub- Eutectic growth (VSS)
0 %
30 %
70 %
100 % Ge
NW: Mean diameter: 19.5nm
NP: Mean diameter: 21.5nm
% of Nanowires
Diameter (nm)
5 nm